Journal of Catalysis 306 (2013) 100–108

Contents lists available at SciVerse ScienceDirect

Journal of Catalysis

journal homepage: www.elsevier.com/locate/jcat

Enhancement of catalytic performance in the benzylation of benzene with benzyl alcohol over hierarchical mordenite

Kunyue Leng [a], Yi Wang [a,c], Changmin Hou [b], Christine Lancelot [c], Carole Lamonier [c], Alain Rives [c], Yinyong Sun [a,*]

[a] School of Chemical Engineering and Technology, Harbin Institute of Technology, Harbin 150001, China
[b] State Key Lab of Inorganic Synthesis and Preparative Chemistry, College of Chemistry, Jilin University, Changchun 130012, China
[c] Unite Catalyse & Chim Solide, UMR8181, Université Science & Technologie Lille, F-59655 Villeneuve Dascq, France

ARTICLE INFO

Article history:
Received 30 May 2013
Revised 2 June 2013
Accepted 7 June 2013
Available online 20 July 2013

Keywords:
Hierarchical
Mesoporous
Mordenite
Benzylation
Treatment
Alkylation

ABSTRACT

Hierarchical mordenites were prepared by a sequential post-treatment method based on a commercial mordenite with a Si/Al molar ratio of 15. The mordenite obtained by acid treatment showed much higher catalytic activity than the parent mordenite in the benzylation of benzene with benzyl alcohol, even a little better than that obtained by acid–base treatment. The apparent reaction rate constant for acid-leached mordenite is six times higher than that for HM. Further, the mordenite with acid–base–acid treatment exhibited the highest catalytic activity among these samples. The apparent reaction rate constant for acid–base–acid-leached mordenite is 15 times that for HM and twice that for acid-leached mordenite and acid–base-leached mordenite. This remarkably enhanced catalytic performance should be attributed to more accessible acid sites and much better mass transfer ability from rich mesoporosity in acid–base–acid-leached mordenite.

1. Introduction

The liquid-phase benzylation of aromatic compounds by benzyl chloride or benzyl alcohol is one of the important reactions in organic chemistry, because it can be used to produce diphenylmethane and substituted diphenylmethanes, which are key industrial compounds as pharmaceutical intermediates or fine chemicals [1,2]. Generally, such reactions are carried out in the presence of homogeneous acid catalysts such as $AlCl_3$, $FeCl_3$, and H_2SO_4 [3,4]. However, these catalysts meet some problems, such as corrosion and difficulty in separation and recovery. Therefore, there have been many attempts to replace these homogenous catalysts with heterogeneous solid catalysts [5–8]. Zeolites, as solid catalysts, have been studied in benzylation reactions [9–13] because of their strong acidity, large surface area, and regular porous structure with excellent stability. The results indicate that highly acidic zeolite catalysts show poor reactivity, mainly because of diffusion limitation caused by their microporous networks [9,10].

Recently, hierarchical zeolites have received much attention because they cannot only overcome the diffusion limitation of zeolites on the reaction rate but also maintain stability and strong acidity, like conventional zeolites [14–16]. Several preparative methods have been adopted in the synthesis of hierarchical zeolites with different framework types, such as ZSM-5 [17–22], Beta [19,22], Y [23–25], and SSZ-13 [26]. Of these, the synthesis of hierarchical mordenite is of practical importance because mordenite, with low preparative cost and strong acidity, has been used for hydroisomerization, alkylation, and dewaxing processes in industry. Currently, hierarchical mordenite can be prepared by dealumination with steam and acid [27–33] or desilication with base [34–39]. The studies indicate that dealumination reduces the density of the acidic sites due to the extraction of aluminum from the framework. As a result, the improvement effect of transport ability on catalytic performance is weakened [36]. For example, Boveri et al. showed that the dealuminated catalyst gave a negligibly improved yield of linear alkylbenzene in the alkylation of benzene with ethylene [33]. Van Bokhoven et al. reported that the acid-leached mordenite had a low catalytic activity similar to that of the parent mordenite in the benzylation of benzene with benzyl alcohol [40].

On the other hand, it has been demonstrated that desilication is an efficient route for preparing hierarchical mordenite, with good preservation of the intrinsic acidity [36]. The hierarchical mordenite obtained by desilication exhibited much better catalytic performance than the parent and acid-leached mordenite. However, recent studies suggested that desilication could result in the deposition of part of the Al species on the external surface of the zeolite framework and thus negatively impact catalytic reactivity. After

* Corresponding author. Fax: +86 4006358835 00379.
E-mail address: yysun@hit.edu.cn (Y. Sun).

0021-9517/$ - see front matter © 2013 Elsevier Inc. All rights reserved.
http://dx.doi.org/10.1016/j.jcat.2013.06.004

subsequent acid washing, the deposited Al species could be removed from the external surface. Then, the catalytic performance could be further improved due to enhanced accessibility [39].

In the present work, with the aim of obtaining a highly efficient catalyst for Friedel–Crafts alkylation based on mordenite, we prepared hierarchical mordenites by a sequential post-treatment method based on a commercial mordenite. Considering that benzyl alcohol is a relatively friendly benzylation reagent due to water as the byproduct, the benzylation of benzene with benzyl alcohol was chosen to evaluate the catalytic performance over the catalysts obtained in each step. The relationship between the structural properties and the catalytic performance will be discussed.

2. Experimental

2.1. Materials

Commercial mordenite was purchased from the Catalyst Plant of Nankai University. HNO_3, NaOH, NH_4NO_3, benzene, and benzyl alcohol were purchased from Sinopharm Chemical Reagents Co. and used without further purification.

2.2. Preparation of catalysts

The commercial mordenite was ion-exchanged with a solution of 1 M NH_4NO_3 at 353 K for 1 h, under stirring with a speed of 1000 rpm, followed by calcination at 823 K for 3 h. The obtained sample was labeled HM.

The HM sample was refluxed with a solution of 2 M HNO_3 at 373 K for 2 h with a liquid-to-solid ratio of 20 ml/g, under stirring with a speed of 1000 rpm. Then, the solid sample was filtered, washed with deionized water, dried at 393 K for 12 h, and ion-exchanged thrice with a solution of 1 M NH_4NO_3 at 353 K for 1 h, followed by calcination at 823 K for 3 h. The final product was labeled HM-A.

The HM-A sample was treated with a solution of 0.2 M NaOH with a liquid-to-solid ratio of 20 ml/g at 343 K for 0.5 h under stirring with a speed of 1000 rpm. The product was filtered, washed with deionized water, dried, ion-exchanged, and then calcined at 823 K for 3 h. The obtained sample was called HM-AB.

The HM-AB sample was treated with a solution of 0.2 M HNO_3 at 323 K for 1.5 h with a liquid-to-solid ratio of 20 ml/g, under stirring with a speed of 1000 rpm. The product was ion-exchanged as described above, followed by calcination at 823 K for 3 h to obtain the sample labeled HM-ABA.

The reused catalyst was obtained by filtering the catalyst after use from the reaction solution, drying, and then calcining at 823 K for 5 h.

2.3. Catalyst characterization

Powder X-ray diffraction (XRD) patterns were recorded on a Rigaku D/Max-2550 diffractometer equipped with a SolX detector—Cu $K\alpha$ radiation with a wavelength of $\lambda = 1.5418$ Å. Relative crystallinity was calculated by the summed intensities of the (330), (150), (202), (350), and (511) reflections. The parent mordenite was assigned a crystallinity of 100%. The crystalline size was determined from the characteristic peak ($2\theta = 22.1^\circ$ for the (150) reflection) using Scherrer's equation, $D = K\lambda/\beta \cos\theta$, where $K = 0.9$, D represents crystallite size, λ represents the wavelength of Cu $K\alpha$ radiation, and β represents the corrected half width of the diffraction peak. SEM images were recorded on a SUPRA 55 operated with an acceleration voltage of 200 kV. Transmission electron microscopy (TEM) images were recorded on a JEOL 2010 with an acceleration voltage of 200 kV. Nitrogen sorption isotherms were obtained at 77 K on a Micromeritics TriStar II 3020 gas sorption and porosimetry system. Samples were normally prepared for measurement after degassing at 423 K under vacuum until a final pressure of 1×10^{-3} Torr was reached. ^{27}Al MAS NMR experiments were performed at room temperature on a Bruker Advance AMS-400 spectrometer at a spinning rate of 12 kHz using a 4-mm probe. In ^{27}Al MAS NMR, a single pulse length of $\pi/6$ and a relaxation delay of 1 s were used, while in ^{29}Si MAS NMR, a high-powered decoupling pulse sequence and a relaxation delay of 6 s were used. The ^{27}Al chemical shift was referenced to (NH_4)-$Al(SO_4)_2{\cdot}12H_2O$ and the ^{29}Si MAS NMR chemical shift to octakis-(trimethylsiloxy)silsesquioxane. X-ray photoelectron spectroscopy (XPS) data were collected on an ESCALAB 250 X-ray photoelectron spectroscope, using Mg $K\alpha$ X-rays as the excitation source. All binding energies were referenced to C1s of 284.6 eV. Temperature-programed desorption of NH_3 (NH_3 TPD) was carried out on a FINESORB-3010 equipped with a thermal conductivity detector. The samples were first outgassed at 823 K for 1 h before the measurement. After being cooled to 303 K, the samples were saturated in an NH_3 stream (5% in Ar) for 1 h and consequently treated in Ar (30 ml/min) for 2 h to remove physisorbed NH_3. Finally, the TPD profile was determined by increasing temperature from 303 to 873 K at a heating rate of 5 K/min while recording NH_3 desorption with a thermal conductivity detector. The adsorption of benzene was performed in an Intelligent Gravimetric Analyzer (IGA-001, Hiden Isochema). Prior to analysis, the powder samples (60–70 mg) were outgassed in situ at 573 K for 4 h under vacuum. When the desired temperature of an experiment was stabilized, the sample was subjected to a pressure step of benzene vapor and the weight change was recorded continuously until equilibrium was reached.

2.4. Catalytic tests

The liquid-phase benzylation of benzene with benzyl alcohol (BA) was carried out in a three-necked round-bottom flask equipped with a reflux condenser and heated in a temperature-controlled oil bath under atmospheric pressure. In a typical run, 14 ml of benzene was added to the catalyst, which had been activated at 773 K in air for 5 h before its use in the reaction. The reaction mixture was maintained for 30 min at the required reaction temperature and then 0.2 ml of benzyl alcohol was added. This moment was regarded as the initial reaction time. Liquid samples were withdrawn at regular intervals and analyzed by gas chromatography on an Agilent 7890A GC with an FID detector using a 30-m packed HP5 column. The products were also identified by GC–MS (5975C-7890A) analysis. Since benzene was in excess, conversion was calculated based on the benzylating reagent, i.e., BA. The selectivity to the product diphenylmethane (DPM) was expressed as the amount of particular product divided by the amount of total products and multiplied by 100.

3. Results and discussion

3.1. Characterization of catalyst

The powder XRD patterns (Fig. 1) of all the samples exhibited well-resolved diffraction peaks, which are characteristic of the mordenite framework structure. Notably, the crystallinity (99%) of HM-A (Table 1) showed a slight decrease from that of HM, although the Si/Al molar ratio increased from 15 to 30 (Table 2). That means that dealumination had a minor influence on the crystallinity of mordenite. A similar result was also observed by another research group [39]. However, after base treatment, the

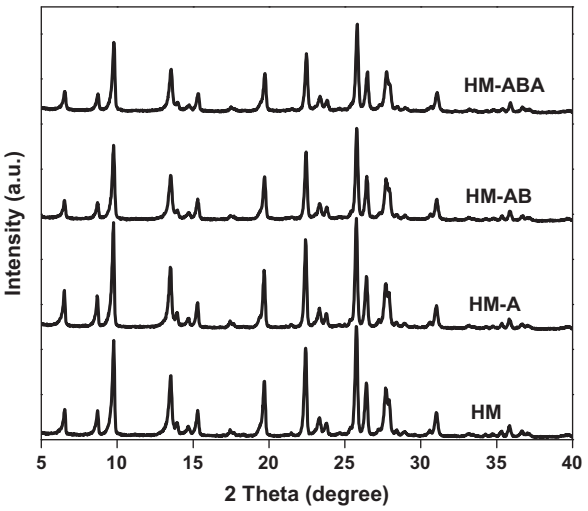

Fig. 1. XRD patterns of various samples.

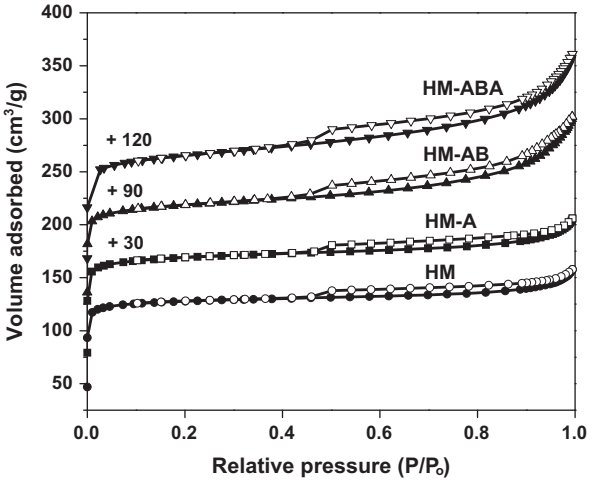

Fig. 2. N_2 adsorption–desorption isotherms of various samples.

crystallinity decreased to 82%. Obviously, the effect of desilication on the crystallinity was relatively large. Further, the acid-washing step resulted in a minor decrease in the crystallinity (75%). These results indicated that the post-treatments could lead to crystallinity loss but the long-range crystal ordering in these samples may be kept. The effect of disilication on crystallinity is greater than that of dealumination. Additionally, by Scherrer's equation, the crystalline sizes of various samples were determined (Table 1). The crystalline sizes of HM, HM-A, HM-AB, and HM-ABA are 449, 424, 401, and 386 nm, respectively. Apparently, the post-treatments resulted in a reduction of crystalline size. Possibly, this is because aluminum and silicon were extracted during leaching, and many cracks and faults were formed on the outer surfaces of zeolite grains, which led to partial collapse of large particles into small particles [40].

The N_2-sorption isotherms of all the samples are shown in Fig. 2. Surprisingly, the parent mordenite HM displayed a hysteresis loop in sorption isotherms, like the treated samples, which suggested the presence of mesopores. For this reason, it may be explained by mesopores in HM being formed by stacking between crystal particles. Generally, commercially available mordenite crystallites have typical dimensions between 100 and 200 nm and form larger particles [39]. In this work, the commercial mordenite used had a crystal size of around 400 nm (Fig. 3). The aggregates of such particles probably resulted in the formation of intercrystalline mesopores. However, the extent of mesoporosity is low. The mesopore volume for HM is 0.1 cm^3/g, which is lower than that for the treated samples (Table 1). The acid-leaching step can improve mesopore volume to some extent, but the enhancement is not significant. Obviously, the mordenite with base treatment had a relatively high mesopore volume. The mesopore volume for HM-AB and HM-ABA is 0.21 and 0.32 cm^3/g, respectively, which is twice and three times that of the parent mordenite. Additionally, all the treated mordenite had a higher BET special surface area and external surface area than the parent mordenite, which should be attributed mainly to the enhancement of porosity

Table 1
N_2 sorption data of various samples.

Sample	BET surface area (m^2/g)	External surface area (m^2/g)[a]	Mesopore surface area (m^2/g)[b]	Micropore volume (cm^3/g)[a]	Mesopore volume (cm^3/g)[b]	Crystalline size (nm)[c]	Crystallinity (%)
HM	398	36	49	0.22	0.10	449	100
HM-A	479	49	66	0.24	0.14	424	99
HM-AB	434	58	102	0.23	0.21	401	82
HM-ABA	470	119	151	0.22	0.32	386	75

[a] *t*-Plot method.
[b] BJH method (adsorption branch).
[c] XRD.

Table 2
Textural properties and chemical composition of various catalysts and the catalytic reaction data.

Sample	Si/Al[a]	NH_3 chemisorbed (mmol/g)[b]	Conversion of BA (%)[c]	Apparent reaction rate constant, k_a ($\times 10^3$ min^{-1})	TOF (s^{-1})
HM	15	1.92	6.1	3.2	0.07
HM-A	30	1.32	40.2	20.9	1.42
HM-AB	20	1.10	28.8	20.2	0.46
HM-ABA	31	1.22	99.6	45.8	3.92

[a] XPS analysis.
[b] NH_3 TPD.
[c] Reaction conditions: amount of catalyst = 0.1 g; benzene = 14 ml; benzyl alcohol = 0.2 ml; reaction temperature = 353 K; reaction time = 0.5 h. The conversion of HM and HM-AB at 0.5 h was estimated according to the curve of conversion with reaction time.

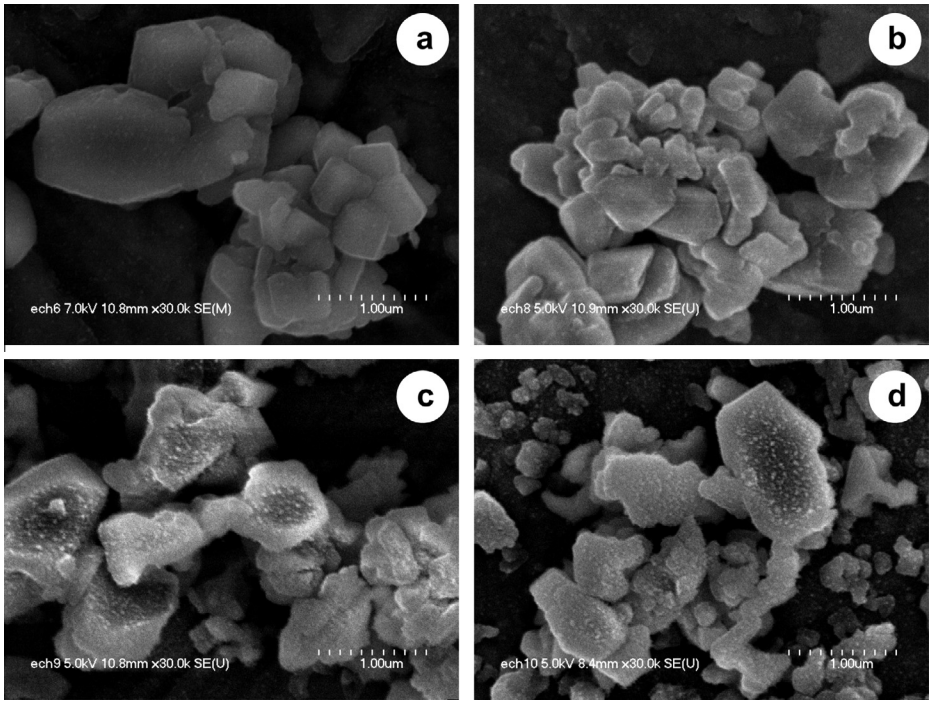

Fig. 3. SEM images of HM (a), HM-A (b), HM-AB (c), and HM-ABA (d).

by the additional mesopores (Table 1). HM-ABA had the highest external surface area (119 m^2/g) among the four samples. The value is more than three times that of HM (36 m^2/g) and more than twice that of HM-A (49 m^2/g) and HM-AB (58 m^2/g). These results indicated that the acid-washing step after base treatment can significantly increase the external surface area. The enhancement should result from the removal of the deposited aluminum species from the surface of framework. Such high mesopore volume and external surface area for HM-ABA would be beneficial for the improvement of mass transfer.

SEM images of all the samples are shown in Fig. 3. Obviously, the parent mordenite had a smooth surface with a prismatic shape. Most of the particle size is between 200 and 400 nm. Some aggregates can be observed, which may explain the reason for mesopore formation in the parent mordenite, as mentioned above. In comparison, for the treated samples, the crystal shape became irregular and crystal size turned small. Moreover, the treated samples had a relatively rough surface. The surface roughness of the samples with base treatment is more visible than that of the acid-leaching sample. These results indicated that the process of post-treatment had an effect on the particle size and morphology of mordenite. TEM images of various samples are shown in Fig. 4. It can be observed that there are intercrystalline mesopores and no intracrystalline mesopores in HM. In contrast, the treated samples displayed the

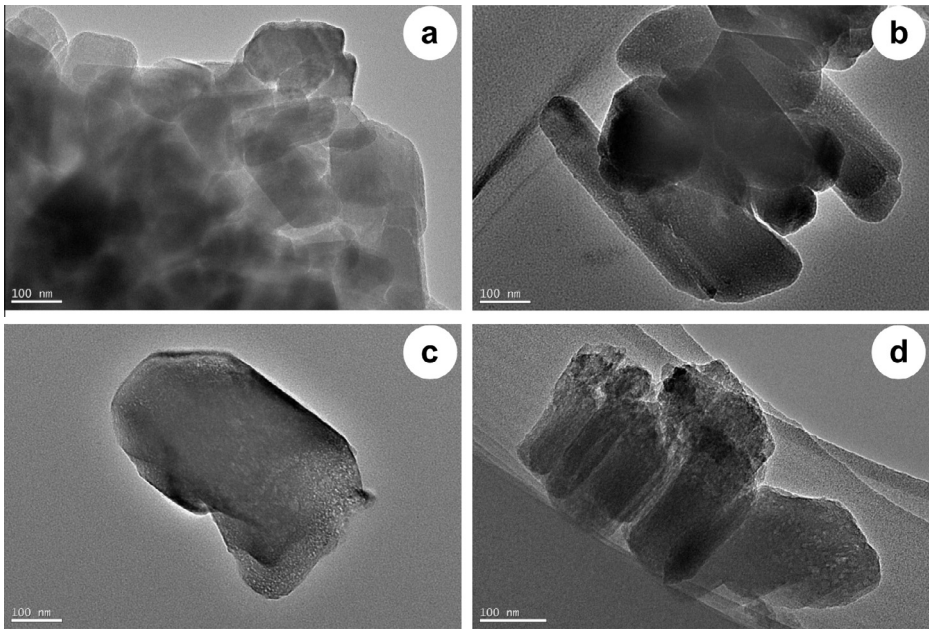

Fig. 4. TEM images of HM (a), HM-A (b), HM-AB (c), and HM-ABA (d).

existence of intracrystalline mesopores. These results are in accordance with the data from N_2 sorption.

To detect the coordination state of aluminum species in the samples, ^{27}Al MAS NMR was done. Fig. 5 shows ^{27}Al MAS NMR spectra of all the samples. Apparently, they exhibited a strong peak centered at around 54 ppm, corresponding to tetrahedrally coordinated aluminum, and a small peak centered at around 0 ppm, corresponding to octahedrally coordinated aluminum, indicating that Al coordination in all the samples was mainly tetrahedral with a small amount octahedral. Additionally, it can be noted that for the treated samples, the peak corresponding to tetrahedrally coordinated aluminum became wide and the total peak area turned small compared with that for the parent mordenite. This suggested that the Al content in the treated samples decreased and some Al sites in the mordenite framework might be slightly changed. Obviously, the resonance peak area of HM-AB is larger than that of HM-A and HM-ABA, indicating that the Al content in HM-AB is higher than that in HM-A and HM-ABA. These results are in agreement with the measurement results of the Si/Al molar ratio (Table 2).

To further uncover the structural changes, the experiments of ^{29}Si MAS NMR for various samples have been done. As can be seen in Fig. 6, the ^{29}Si MAS NMR of all the samples is mainly composed of different tetrahedral sites. The deconvolution of ^{29}Si spectrum led to six peaks centered at −97 to −103 ppm (SiOH), −106.25, and −110.08 ppm (Si(3Si, 1Al)), and −112.82 and −115.30 ppm (Si(4Si)), respectively. When the proportions of different Si sites are compared, it can be found that acid leaching obviously removed the Al species in the framework because the proportion of Si(3Si, 1Al) decreased from 31.39 to 23.43%. Further, the desilication almost did not change the proportion of Si(4Si) and Si(3Si, 1Al). Generally, it is thought that during desilication, the Si species such as Si(4Si) can easily be leached out and it is difficult to remove the Si species such as Si(3Si, 1Al) because the negatively charged AlO_4^- tetrahedra prevent the hydrolysis of the Si–O–Al bond in the presence of OH^- [41]. In this case, if the desilication process only removed the Si species such as Si(4Si) and SiOH in HM-A, the proportion of Si(3Si, 1Al) sites should increase. However, the fact is that the proportion of Si(4Si) and Si(3Si, 1Al) in HM-A and HM-AB is almost the same, suggesting that the base treatment should result in partial loss of framework Al species. Possibly, this part of Al species existed in HM-AB as extra-framework Al. After the final acid-washing step, they could be removed. The fact that the proportion of SiOH, Si(3Si, 1Al), and Si(4Si) sites in HM-ABA is very close to that in HM-AB and the Si/Al molar ratio increased from 20 to 31 could support this opinion.

The acidity of the samples was characterized by NH_3 TPD. As can be seen in Fig. 7, all the samples showed two desorption peaks of NH_3 in the range 303–773 K. These desorption peaks corresponded to two different type of acid sites. The low-temperature desorption peak (303–523 K) was attributed to weak acid sites, and the high-temperature desorption peak (523–773 K) was due to NH_3 bound to strong acid sites. The total number of acid sites listed in Table 2 was calculated by peak area of desorbed NH_3. The number of acid sites was 1.92 mmol/g for HM, 1.32 mmol/g for HM-A, 1.1 mmol/g for HM-AB, and 1.22 mmol/g for HM-ABA, respectively. Notably, HM possessed more acid sites than the treated samples, because HM had a lower Si/Al molar ratio (Si/Al = 15). Particularly, HM-AB (Si/Al = 20) exhibited fewer acid sites than HM-A and HM-ABA, although it had a lower Si/Al molar ratio than HM-A (Si/Al = 30) and HM-ABA (Si/Al = 31). Possibly, the deposition of partial Al species on the mordenite framework after the desilication made some acid sites inaccessible. This fact that the

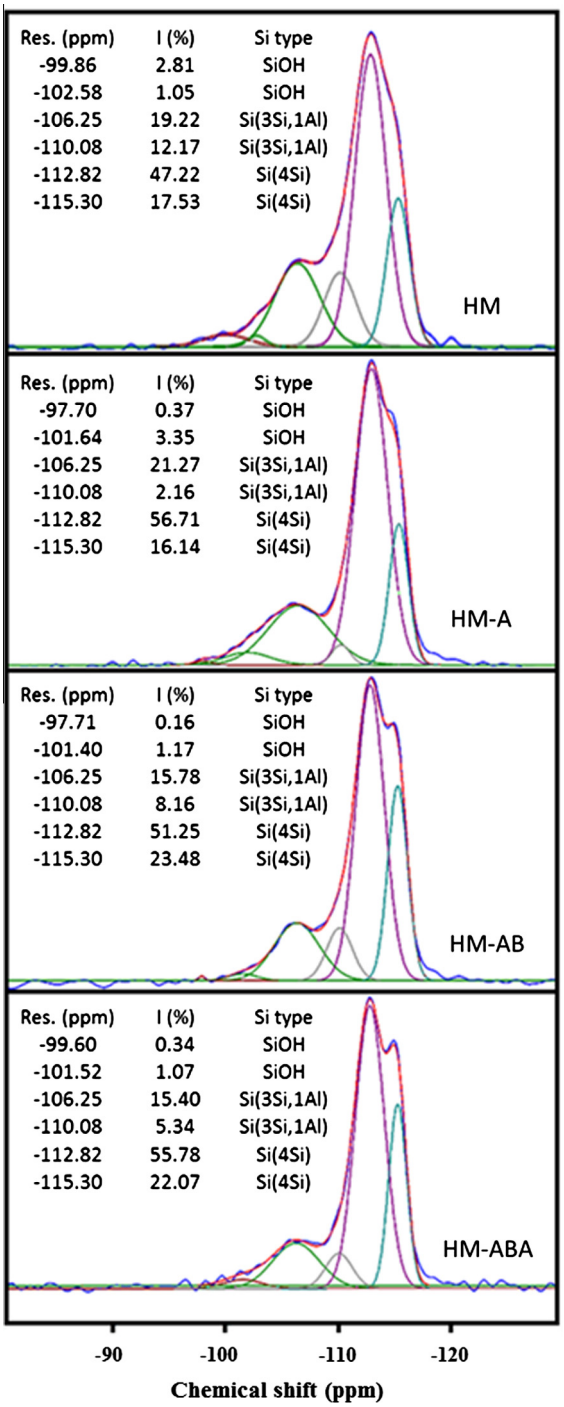

Fig. 6. ^{29}Si NMR spectra of various samples.

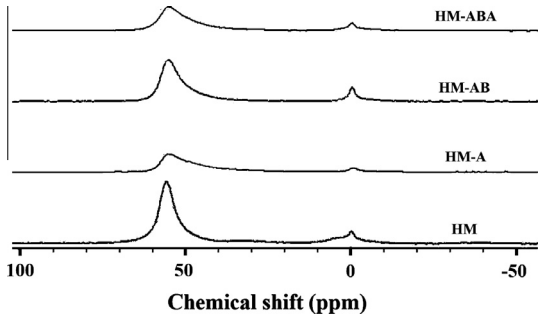

Fig. 5. ^{27}Al NMR spectra of various samples.

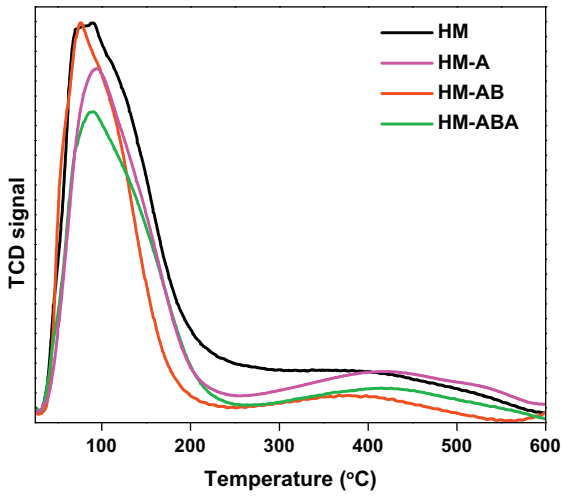

Fig. 7. NH_3 TPD profiles of various samples.

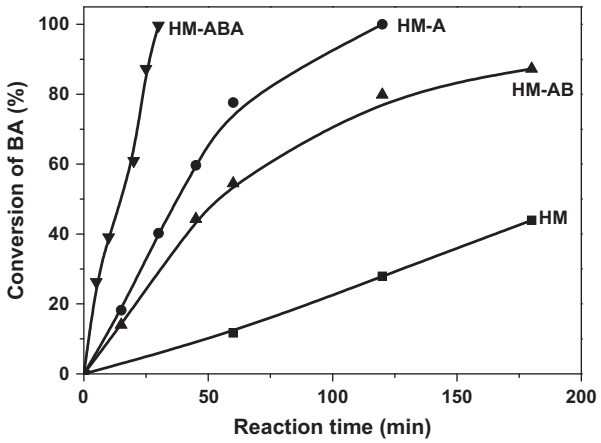

Fig. 8. Catalytic activities of various catalysts in the benzylation reaction of benzene with benzyl alcohol at 353 K.

acid-washing step increased the number of acid sites could be a proof of this supposition.

3.2. Catalytic activity

To evaluate the catalytic performance of these catalysts, the benzylation of benzene with benzyl alcohol was first chosen at a reaction temperature of 353 K. The reaction pathway in the benzylation is displayed in Scheme 1. The products in the reaction are mainly diphenylmethane (DPM) and dibenzyl ether (DBE). The product DBE can be further converted into DPM. Meanwhile, the polyalkylated products may be formed by the benzylation of DPM.

The conversion of benzyl alcohol with reaction time over various catalysts is shown in Fig. 8. Obviously, HM gave a low catalytic activity, with a BA conversion of 6.1% after a reaction time of 0.5 h (Table 2). Interestingly, HM-A gave much higher catalytic activity than HM. The BA conversion reached 40.2% after a reaction time of 0.5 h, even a little better than that of HM-AB (28.8%). This result is different from the previous report from van Bokhoven's group [40]. They showed that acid-leaching mordenite gave a very low catalytic activity, similarly to the parent mordenite, and a much lower catalytic activity than the acid–base-leaching mordenite. This difference might be due to the use of different parent mordenite. In that work, the used mordenite had a plate-like morphology and a large crystal size (around 5 μm). In comparison, in this work, the commercial mordenite had a prismatic morphology and a small crystal size (around 400 nm). However, further study was required to make the reason clear. Importantly, HM-ABA exhibited remarkably enhanced catalytic activity, which almost ended this reaction after a reaction time of 0.5 h. The apparent reaction rate constant for HM-ABA is 15 times that for HM and twice that for HM-A and HM-AB (Table 2). Additionally, the turnover frequency (TOF) has been estimated based on the mole number of diphenylmethane produced per mole Al per second. The value of TOF was 0.07 s^{-1} for HM, 1.42 s^{-1} for HM-A, 0.46 s^{-1} for HM-AB, and 3.93 s^{-1} for HM-ABA, respectively (Table 2). Based on the comparison of TOF data, it can be seen that the enhancement of catalytic performance is much greater. For example, the TOF of HM-ABA is 50 times higher than that of HM, twice that of HM-A, and eight times that of HM-AB. However, as far as the selectivity is concerned, all the catalysts are similar. The obtained products contained mainly DPM (above 95%) with a small amount of DBE (below 5%). No polyalkylated products were detected.

In comparison with previous reports on mesoporous zeolites in the benzylation of benzene alcohol with benzene, HM-ABA is a highly efficient catalyst. For example, Prins et al. showed that mesoporous ZSM-5 prepared by a soft-template method took 10 h to end this reaction at the same reaction temperature [42]. Van Bokhoven et al. displayed that mesoporous mordenite obtained by an acid–base-leaching method completed the reaction after 3 h [40]. Ryoo et al. reported that an ordered mesoporous zeolite MMS gave a BA conversion of 44% with a DMP selectivity of 77% and a disordered mesoporous Beta showed a BA conversion of 33% with a DMP selectivity of 68% after 5 h at the same reaction temperature [22]. Although in the above works the amounts of catalyst and benzyl alcohol are different from those used in this work, it can be estimated that HM-ABA is still a very active catalyst in

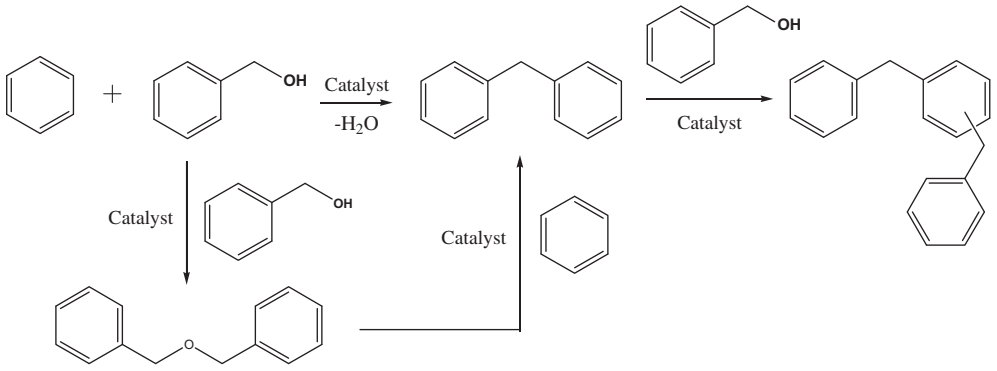

Scheme 1. Benzylation reaction pathway of benzene with benzyl alcohol.

this reaction after the effect factor of amounts of catalyst and benzyl alcohol is deducted.

To find why HM-ABA exhibited remarkably enhanced catalytic activity in the reaction, the relationship between catalytic performance and structural properties needs to be considered. In general, it is thought that the benzylation reaction proceeds via an electrophilic intermediate involving the interaction of benzyl alcohol with the acid sites. The acid sites polarize the benzylating agent and in turn produce an electrophile. Then, the generated electrophilic species attack the benzene ring, resulting in the formation of DPM [9,43]. Therefore, the number of acid sites is an important factor that affects catalytic activity. However, it can be noted that HM had the largest total number of acid sites but exhibited the lowest catalytic activity among the four samples and HM-ABA possessed a similar total number of acid sites to HM-A but showed much higher catalytic activity than HM-A (Table 2). These results indicated that the total number of acid sites had no good relationship with catalytic activity. Possibly, the accessibility of acid sites played a vital role in this reaction. Nevertheless, the characterization of accessible acid sites is not easy. Although an accessibility index derived from infrared spectroscopy of substituted alkylpyridines with different sizes has been proposed to characterize the accessibility of acid sites in hierarchical zeolites, and this method has been demonstrated to be efficient over hierarchical ZSM-5 [44], its applicability to other types of zeolites needs to be further investigated. Recently, Park et al. measured the number of external acid sites in mesoporous ZSM-5 by the chemisorption of 2,6-di-*tert*-butylpyridine and found that mesoporous ZSM-5 with more external acid sites exhibited superior catalytic performance in the benzylation of aromatics with benzyl alcohol [45].

On the other hand, mass transfer ability is another important factor that influences catalytic performance. It is well known that the micropore system of mordenite consists of a 12-membered ring (MR) pore channel of 0.67 × 0.70 nm and an 8-MR side pocket of 0.34 × 0.48 nm. Generally, mordenite is considered a one-dimensional pore system due to inaccessibility of the 8-MR pores for most molecules [39]. In the benzylation reaction, the molecular size of reactants and products is around 0.5 nm, which is close to the size of the pore channel with 12-MR and larger than that of the pore channel with 8-MR [45]. Obviously, such a pore system is not beneficial for mass transfer. Additional mesoporosity and external surface area can improve the ability for mass transfer. As listed in Tables 1 and 2, the treated samples with higher mesopore volume and external surface area had a much higher catalytic activity than the parent mordenite. HM-ABA, with the highest external surface area and mesopore volume, exhibited the best catalytic activity. These results seemed to reveal that the catalytic performance had a close relationship with the mass transfer ability. However, HM-A especially had a lower mesopore volume and external surface area than HM-AB but showed slightly better catalytic activity, probably because the deposited Al species after desilication blocked partial pore channels and covered some acid sites, and as a result, partial acid sites in HM-AB are inaccessible.

To demonstrate that the sample with large external surface area and mesopore volume had better mass transfer ability, the diffusion experiments were carried out by the adsorption of benzene at 298 K and 0.1 bar. The adsorbed amount of benzene at adsorption equilibrium is 27.4 mg/g for HM, 38.6 mg/g for HM-A, 53.5 mg/g for HM-AB, and 62.6 mg/g for HM-ABA (Table 3). The normalized uptake curves of various samples are shown in Fig. 9. The effective diffusivity was calculated according to the reported method [46]. The values for HM, HM-A, HM-AB, and HM-ABA are 1.93×10^{-20}, 2.76×10^{-20}, 5.98×10^{-20}, and 6.93×10^{-20} m^2/s, respectively (Table 3), which increased with the mesopore volume and external surface area. Among these samples, HM-ABA had the highest effective diffusivity, which is three times larger than HM. These results are in good agreement with our supposition. Based on the above analysis, it can be concluded that a highly efficient catalyst in this reaction should have a good combination of the number of accessible acid sites, mesopore volume, and external surface area. The catalyst with more accessible acid sites, larger mesopore volume, and greater external surface area can be catalytically more active in this reaction. Therefore, such outstanding catalytic performance over HM-ABA catalyst should be attributed to more accessible acid sites and much better mass transfer ability from rich mesoporosity in HM-ABA.

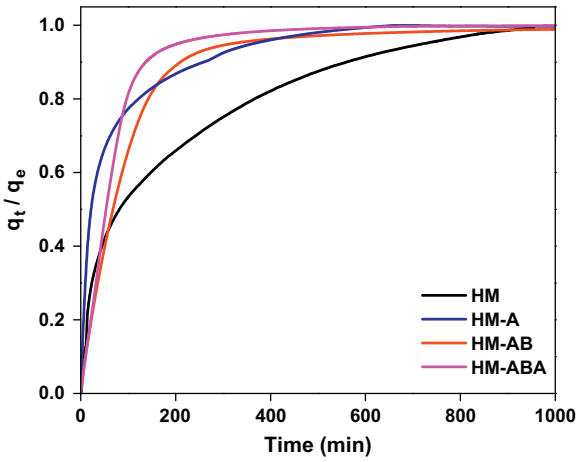

Fig. 9. Diffusion curves of benzene in various samples.

To further investigate the catalytic reactivity of HM-ABA, the effect of reaction temperature was tested. As shown in Fig. 10, reaction temperature had a strong effect on BA conversion. For example, at 343 K, the BA conversion was 40% after a reaction time of 0.5 h, while at 353 K, the BA conversion reached nearly 100%. The rate data for the benzylation of benzene in excess of benzene

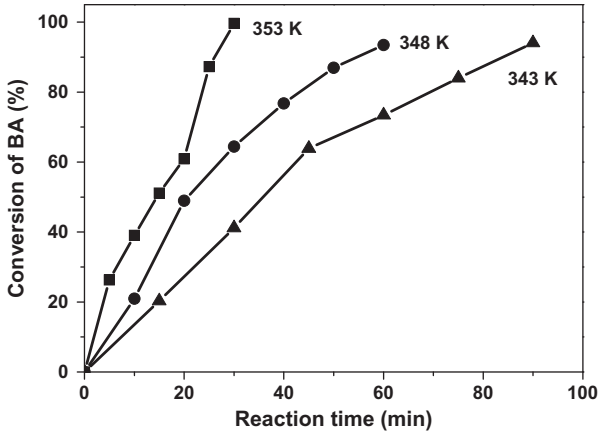

Fig. 10. Effect of reaction temperature on the benzylation reaction of benzene with benzyl alcohol over HM-ABA catalyst.

Table 3
Adsorbed amount at adsorption equilibrium and diffusivity of benzene at 298 K and 0.1 bar on various samples.

Sample	Adsorption amount (mg/g)	Diffusivity (10^{-20} m^2/s)
HM	27.4	1.93
HM-A	38.6	2.76
HM-AB	53.5	5.98
HM-ABA	62.6	6.93

over HM-ABA catalyst could be well fitted to a pseudo-first-order rate law, $\ln(1/1-x) = k_a(t-t_0)$, where k_a is the apparent rate constant, x is the fractional conversion of benzyl alcohol, t is the reaction time, and t_0 is the induction period corresponding to the time required to reach equilibrium temperature. A linear plot of $\log(1/1-x)$ versus $t-t_0$ can be obtained. The reaction rate became high with increasing temperature. At 343 K, the apparent rate constant k_a was 2.23×10^{-4} min^{-1}, while at 348 K it reached 3.54×10^{-4} min^{-1}, which is nearly 1.6 times that at 343 K. Further increase in temperature to 353 K increased k_a to 4.58×10^{-4} min^{-1}, twice as high as at 343 K. These first-order rate constants gave a linear Arrhenius plot (Fig. 11) with an estimated activation energy of 74 kJ/mol for the HM-ABA catalyst. This value is much lower than that of the reported mesoporous ZSM-5 [42].

3.3. Reusability of the catalyst

The reusability of heterogeneous catalysts is one of their main advantages. To test its reusability, a reaction using the HM-ABA catalyst was carried out at 353 K. Fig. 12 shows the catalytic activities of fresh and reused HM-ABA in the benzylation of benzene by benzyl alcohol. The fresh catalyst gave an activity of 15.3 mmol/g at a reaction time of 0.5 h. Correspondingly, the first and second reused catalysts presented an activity of 15.2 and 15.4 mmol/g, respectively. These results indicate that the catalyst could be reused and maintain the initial activity even after three cycles. Such catalytic performance is of great importance for potential industrial application.

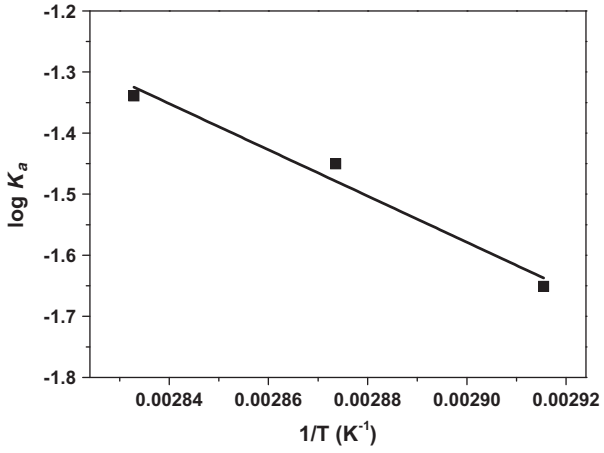

Fig. 11. Arrhenius plot of log k_a as a function of $(1/T)$ for the benzylation reaction of benzene with benzyl alcohol over HM-ABA catalyst.

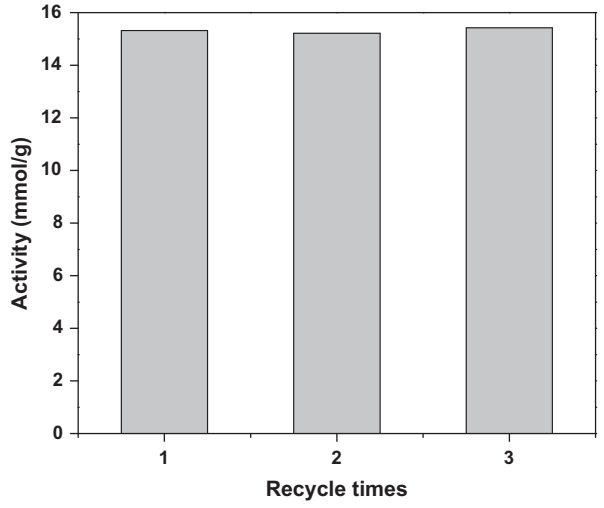

Fig. 12. Reusability of HM-ABA in the benzylation reaction of benzene with benzyl alcohol at 353 K. Reaction conditions: amount of catalyst = 0.2 g; benzene = 28 ml; benzyl alcohol = 0.4 ml, reaction time = 0.5 h.

4. Conclusions

Hierarchical mordenites were prepared by a sequential post-treatment method based on a commercial mordenite. The hierarchical mordenite obtained by acid–base–acid treatment exhibited remarkably enhanced catalytic activity in the benzylation of benzene with benzyl alcohol. The apparent reaction rate constant is 15 times that for the parent mordenite and twice that for the acid-leaching mordenite and base-leaching mordenite. Such outstanding catalytic performance should be attributed to more accessible acid sites and much better mass transfer ability from rich mesoporosity in HM-ABA. The activation energy for HM-ABA in this reaction is calculated with a low value of 74 kJ/mol. Additionally, the catalyst HM-ABA could be reused and almost maintain the initial activity even after several cycles. These results indicate that hierarchical mordenites have potential applications in Friedel–Crafts alkylation.

Acknowledgments

The project was sponsored by Scientific Research Starting Funding from Harbin Institute of Technology, Open Funding from the State Key Lab of Inorganic Synthesis and Preparative Chemistry, Jilin University, and the Scientific Research Foundation for Returned Overseas Chinese Scholars, State Education Ministry. We thank Professor Shuxia Liu and Xingquan Wang from Northeast Normal University for the diffusion measurements.

References

[1] G.A. Olah, Friedel-Crafts and Related Reactions, Wiley-Interscience, New York, 1963.
[2] G.A. Olah, Friedel-Crafts Chemistry, Wiley, New York, 1973.
[3] R. Commandeur, N. Berger, P. Jay, J. Kervenal, European Patent 0422 986, 1991.
[4] I. Iovel, K. Mertins, J. Kischel, A. Zapf, M. Beller, Angew. Chem. Int. Ed. 44 (2005) 3913.
[5] J. Chiu, D. Pine, S. Bishop, B. Chmelka, J. Catal. 221 (2004) 400.
[6] K. Bachari, J. Millet, B. Benaïchouba, O. Cherifi, F. Figueras, J. Catal. 221 (2004) 55.
[7] N.B. Shrigadi, A.B. Shinde, S.D. Samant, Appl. Catal. A Gen. 252 (2003) 23.
[8] S.K. Jana, Catal Surveys Asia 9 (2005) 25.
[9] B. Coq, V. Gourves, F. Figueras, Appl. Catal. A Gen. 100 (1993) 69.
[10] V.R. Choudhary, S.K. Jana, B.P. Kiran, Catal. Lett. 59 (1999) 217.
[11] G. Winé, J. Matta, J.P. Tessonnier, C. Pham-Huu, M.-J. Ledoux, Chem. Commun. (2003) 530.
[12] V.D. Chaube, Catal. Commun. 5 (2004) 321.
[13] N. Candu, M. Florea, S.M. Coman, V.I. Parvulescu, Appl. Catal. A Gen. 393 (2011) 206.
[14] J. Pérez-Ramírez, C.H. Christensen, K. Egeblad, C.H. Christensen, J.C. Groen, Chem. Soc. Rev. 37 (2008) 2530.
[15] R. Chal, C. Gérardin, M. Bulut, S. van Donk, ChemCatChem 3 (2011) 67.
[16] D.P. Serrano, J.M. Escola, P. Pizarro, Chem. Soc. Rev. 42 (2013) 4004.
[17] C.J.H. Jacobsen, C. Madsen, J. Houzvicka, I. Schmidt, A. Carlsson, J. Am. Chem. Soc. 122 (2000) 7116.
[18] M. Ogura, S. Shinomiya, J. Tateno, Y. Nara, E. Kikuchi, M. Matsukata, Chem. Lett. 29 (2000) 882.
[19] F.-S. Xiao, L. Wang, C. Yin, K. Lin, Y. Di, R. Xu, D.S. Su, R. Schlögl, T. Yokoi, T. Tatsumi, Angew. Chem. Int. Ed. 45 (2006) 3090.
[20] M. Choi, H. Cho, R. Srivastava, C. Venkatesan, D. Choi, R. Ryoo, Nat. Mater. 5 (2006) 718.
[21] H. Wang, T.J. Pinnavaia, Angew. Chem. Int. Ed. 45 (2006) 7603.
[22] K. Na, C. Jo, J. Kim, K. Cho, J. Jung, Y. Seo, R.J. Messinger, B.F. Chmelka, R. Ryoo, Science 333 (2011) 328.
[23] Z. Qin, B. Shen, X. Gao, F. Lin, B. Wang, C. Xu, J. Catal. 278 (2011) 266.
[24] D. Verboekend, G. Vilé, J. Pérez-Ramírez, Adv. Funct. Mater. 22 (2012) 916.

[25] Z. Qin, B. Shen, Z. Yu, F. Deng, L. Zhao, S. Zhou, D. Yuan, X. Gao, B. Wang, H. Zha, H. Liu, J. Catal. 298 (2013) 102.
[26] L. Wu, V. Degirmenci, P. Magusin, N. Lousberg, E. Hensen, J. Catal. 298 (2013) 27.
[27] G.S. Lee, J.J. Maj, S.C. Rocke, J.M. Garcés, Catal. Lett. 2 (1989) 243.
[28] R.A. Beidin, C. Choi-Feng, J.B. Hall, B.J. Huggins, G.J. Ray, Top. Catal. 4 (1997) 27.
[29] S. Bernasconi, J.A. van Bokhoven, F. Krumeich, G.D. Pringruber, R. Prins, Micropor. Mesopor. Mater. 66 (2003) 21.
[30] M. Boveri, C. Márquez-Álvarez, M.Á. Laborde, E. Sastre, Catal. Today 114 (2006) 217.
[31] K.-H. Lee, B.-H. Ha, Micropor. Mesopor. Mater. 23 (1998) 211.
[32] R. Giudici, H.W. Kouwenhoven, R. Prins, Appl. Catal. A Gen. 203 (2000) 101.
[33] K.H. Chung, Micropor. Mesopor. Mater. 111 (2008) 544.
[34] J.C. Groen, L.A.A. Peffer, J.A. Moulijn, J. Pérez-Ramírez, Micropor. Mesopor. Mater. 69 (2004) 29.
[35] X.T. Wei, P.G. Smirniotis, Micropor. Mesopor. Mater. 97 (2006) 97.
[36] J.C. Groen, T. Sano, J.A. Moulijn, J. Pérez-Ramírez, J. Catal. 251 (2007) 21.
[37] V. Paixão, A.P. Carvalho, J. Rocha, A. Fernandes, A. Martins, Micropor. Mesopor. Mater. 131 (2010) 350.
[38] A.N.C. van Laak, R.W. Gosselink, R.L. Sagala, J.D. Meeldijk, P.E. de Jongh, K.P. de Jong, Appl. Catal. A Gen. 382 (2010) 65.
[39] A.N.C. van Laak, S.L. Sagala, J. Zečević, H. Friedrich, P.E. de Jongh, K.P. de Jong, J. Catal. 276 (2010) 170.
[40] X. Li, R. Prins, J.A. van Bokhoven, J. Catal. 262 (2009) 257.
[41] A. Bonila, D. Baudouin, J. Pérez-Ramírez, J. Catal. 265 (2009) 170.
[42] Y. Sun, R. Prins, Appl. Catal. A Gen. 336 (2008) 11.
[43] A.P. Singh, D. Bhattarchaya, S. Sharma, J. Mol. Catal. 102 (1995) 139.
[44] F. Thibault-Starzyk, I. Stan, S. Abelló, A. Bonilla, K. Thomas, C. Fernandez, J. Gilson, J. Pérez-Ramírez, J. Catal. 264 (2009) 11.
[45] H. Jin, M.B. Ansari, E.-Y. Jeong, S.-E. Park, J. Catal. 291 (2012) 55.
[46] L. Gueudré, M. Milina, S. Mitchell, J. Pérez-Ramírez, Adv. Funct. Mater., 2013. doi:10.1002/adfm.201203557.